




Paper Type: Original Article

# Analyzing the Impact of Sustained Loading and Corrosion on the Structural Integrity of Reinforced Concrete Beams: a Hybrid Neural Network Approach

Alireza Sadighi Agdas<sup>1,\*</sup> , Yousef Zand<sup>2</sup>

<sup>1</sup> Ghateh Gostar Novin Company, Tabriz 51579, Iran; alireza.sadighi.agdas@hotmail.com

<sup>2</sup> Department of Civil Engineering, Tabriz Branch, Islamic Azad University, Tabriz, Iran; zandi@iaut.ac.ir

Citation:

Received: 14 January 2024

Revised: 20 February 2024

Accepted: 10 March 2024

Sadighi Agdas, A., & Zand, Y. (2024). Analyzing the impact of sustained loading and corrosion on the structural integrity of reinforced concrete beams: a hybrid neural network approach. *International journal of researches on civil engineering with artificial intelligence*, 1(4), 59-72.

## Abstract

Deicing chemicals are used in different climates to keep the corrosion process going, and this global examination of the number of defective bridges makes it necessary to develop better analytical techniques for Reinforced Concrete (RC) components that have been corrupted. This research aims to explore the combined effects of prolonged loads and corrosion on the structural function of RC beams. This experimental study examined eight RC beams, including corroded and uncorroded ones, accelerated using impressed current technology. Four-point sustained bending loads applied to all the beams were equal to 16, 32, or 50% of the designed ultimate load, respectively. The degree of corrosion, fracture diameter and patterns, and mid-span beam deflection were measured throughout the test. The experimental tests are analyzed using Finite Element Analysis (FEA), but these studies are expensive, time-consuming, and require a high input error percentage. To estimate these inputs, a new Neural Network (NN) model as a hybrid of an Artificial Neural Network (ANN) and a Support Vector Machine (SVM) has been constructed in this study based on data from the literature. In addition to the hybrid's superior performance, it was discovered that the corrosion level influenced the beams to corrode more. In contrast, the beams' stiffness of corrosion via the accelerated process declined more rapidly with the same rebar mass loss rate. The main reasons the beams could not hold as much weight were the loss of cross-sectional area and the deterioration of the corroded rebar's mechanical features. Bond loss was mostly to blame for the drop in stiffness.


**Keywords:** Flexural behaviour, Corroded concrete, Beams, Crack, Neural network, ANN-SVM.

## 1 | Introduction

Long-term exposure to a severe climate would reduce the strength of Reinforced Concrete (RC) structures because of steel bar corrosion. Deicing salts and saltwater are primarily responsible for steel bar corrosion in concrete buildings. When the carbonation or chloride ion concentration on a steel surface becomes a

 Corresponding Author: jalireza.sadighi.agdas@hotmail.coma@



 Licensee System Analytics. This article is an open access article distributed under the terms and conditions of the Creative Commons Attribution (CC BY) license (<http://creativecommons.org/licenses/by/4.0>).

threshold amount, the oxide coating may be removed, and corrosion could begin. It is widely known that corrosion products formed at the interface between steel and concrete may cause the concrete cover to expand and finally break. Corrosion can also reduce the cross-sectional area of rebar and significantly impact mechanical properties like elasticity and ultimate strength. It was discovered that the degree of decrease produced from these study operations varied considerably. It was discovered that the accelerated corrosion process, utilized in many experiments, had substantially distinct impacts on the structure of RC components compared to the normal corrosion process [1]. The effects of concrete and steel's deteriorating bond were discussed, reaching a reasonable level of agreement. The modelling considered four factors: corrosion period, beam cross-sectional area, material characteristics, and current density. The results from finite elements have matched experimental data well. The researchers established the suggested damaged bond model's validity in simulating the failure process [2]. One of the most commonly used building materials worldwide is RC. Due to their excellent service performance, RC structures are often considered permanent structures that may be free of serious degradation issues for a long time. One of the main variables generating durability issues for RC constructions is the corrosion of steel bars [3].

On the one hand, corrosion may cause steel bars to lose cross sections and degrade their mechanical characteristics, which lowers a structural member's bearing capacity. Also, corrosion of steel bars may decrease the bonding performance between concrete and steel, leading to a drop in stiffness, which can cause deflection over the service life. In the tests done by Ballim et al. [4], a current density of 400  $\text{IA}/\text{cm}^2$  was applied, which quickly achieved the optimal corrosion degree. Meanwhile, a typical density that controls the corrosion ratio for real concrete buildings eroding in use typically varies between 0.1 and 100  $\text{IA}/\text{cm}^2$  [5], [6]. An empirical evaluation of the behaviour of RC beams exposed to concurrent loading at various levels and reinforcement corrosion at various ratios was conducted for this work. Particular focus was placed on the combined impacts on corrosion crack initiation, propagation, and RC beam deflection. *Fig. 1* shows how reinforcement corrosion seriously undermines the performance of an RC structure.



**Fig. 1. Reinforcement corrosion seriously undermines the performance of an RC structure.**

### 1.1 | Flexural Behavior

A beam acts after it has been loaded to a level of sustained load  $P_{re}$  that is greater than the cracking load  $P_{cr}$ , then unloaded, and then loaded again until it breaks (*Fig. 4*). The slope of Line BE,  $k_a$  is given by *Eq. (1)* [7].

$$k_a = \psi k_e + (1 - \psi) k_g, \tag{1}$$

$$\psi = \frac{(P_y - P_{re})}{(P_y - P_{cr})}.$$

For a beam with small flexural cracks,  $P_{re} \approx P_{cr}$ , the recovery is likely to be full. There is no way for a badly cracked beam,  $P_{re} \approx P_y$ , to get back to its original shape. Inelastic strains recover as the flexural cracks close

up along the unloading between these two cases. *Eq. (1)* is used to figure out how a loading-unloading cycle affects the load-deflection curve of corroded beams that have been under load for a long time.

## 1.2 | Maximum Bond Stress

Kemp and Wilhelm [8] experimented to determine the maximum bond stress of concrete beams reinforced with deformed steel bars. They derived *Eq. (2)* to calculate the maximum bond stress. The maximum bond stress of an uncorroded part of the beam is comprised of two components: the bond strength contributed by the concrete and the bond strength contributed by the stirrups  $\tau_{st}$ . *Fig. 2* depicts the stress and strain distribution of the simply-supported beams section.

$$\tau_{\max v} = \underbrace{\left(0.55 + 0.24 \frac{c_c}{d_b}\right) \sqrt{f'_c}}_{\tau_{\text{conc}}} + \underbrace{0.191 \frac{A_t f_{yt}}{s_s d_b}}_{\tau_{\text{st}}} \quad (2)$$

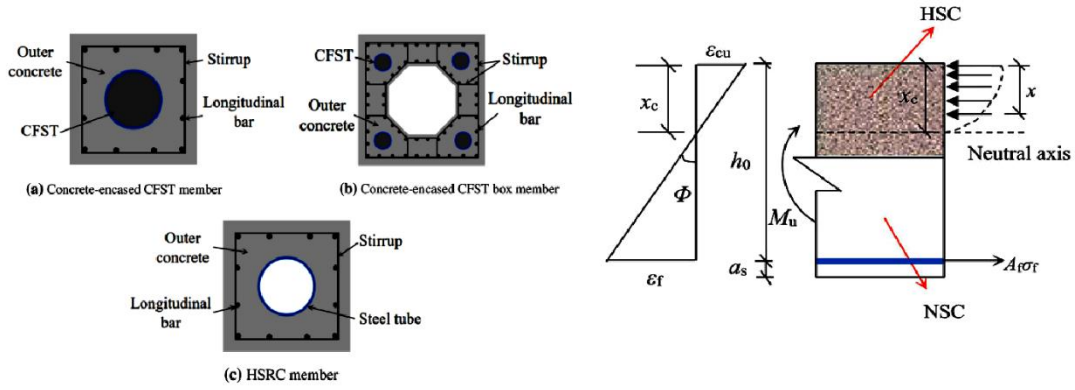


Fig. 2. Simple-supported beam stress-strain distribution.

The benefits of high-strength concrete (HSC) and the economics of normal-strength concrete (NSC) may be combined organically if HSC is used solely in important regions of structural engineering components and NSC is employed in other portions. During pouring, the top of the NSC should stay rough to bond well with the HSC.

### 1.2.1 | Corroded parts of the beam

Saifullah and Clark [9] used experiments to develop a factor called R that can be used to forecast how the bond strength will change when the steel reinforcement rusts. This factor says that the bond will get stronger at first before corrosion cracks it, but it will get weaker as the per cent steel mass loss due to corrosion  $m_1$  increment.

$$R = A_1 + A_2 m_1. \quad (3)$$

*Table 2* shows how the current density used to cause corrosion affects the values of  $A_1$  and  $A_2$ . In general, the stirrups' effect on the bond strength is not influenced by the corrosion level in the flexural reinforcement [10], meaning that corrosion of the flexural reinforcement will not change how much the stirrups add to the bond strength if they are not corroded. So, the maximal bond stress of a part of the beam that has eroded,  $\tau_{\max c}$  can be found by

$$\tau_{\max c} = \frac{(A_1 + A_2 m_1)}{R} \underbrace{\left(0.55 + 0.24 \frac{c_c}{d_b}\right) \sqrt{f'_c}}_{\tau_{\text{conc}}} + \underbrace{0.191 \frac{A_t f_{yt}}{s_s d_b}}_{\tau_{\text{st}}} \quad (4)$$

## 1.3 | Mean Crack Spacing

*Eq. (5)*, provided by the CEB-FIP model code [11], will be utilized to define the mean crack spacing.

$$s_m = 2 \left( C + \frac{s_b}{10} \right) + \kappa_1 \kappa_2 \frac{d_b}{\rho_{ef}} \quad (5)$$

$$\rho_{ef} = A_s/A_{cef}. \quad (6)$$

$$\kappa_1 = \begin{cases} 0.4, & \text{for deformed bars,} \\ 0.8, & \text{for plain bars.} \end{cases} \quad (7)$$

Eq. (7) shows that the coefficient  $\kappa_1$  goes up as the quality of the steel and concrete bond goes down. Here, the coefficient  $\kappa_1$  is changed to  $\kappa_{1m}$  to account for how changing the bond strength affects the average distance between cracks.

$$\kappa_{1m} = 0.4 \frac{\tau_{conc}}{\tau_{maxc}}. \quad (8)$$

The terms  $\alpha_1$  and  $\beta_1$  are expressed as follows [12]:

$$\alpha_1 \beta_1 = \frac{\varepsilon_c}{\varepsilon_{ce}} - \frac{1}{3} \left( \frac{\varepsilon_c}{\varepsilon_{ce}} \right)^2. \quad (9)$$

$$\beta_1 = \frac{4 - \varepsilon_c/\varepsilon_{co}}{6 - 2\varepsilon_c/\varepsilon_{ca}}. \quad (10)$$

Considering Eqs. (9) and (10), equilibrium equations in the pre-yield stage are

$$\alpha_1 f'_c \beta_1 c b + A'_s E_s \frac{\varepsilon_c (c - d')}{c} - E_c b \frac{\varepsilon_c (h - c)^2}{2c} - A_s E_s \frac{\varepsilon_c (d - c)}{c} = 0. \quad (11)$$

$$\alpha_1 f'_c \beta_1 c b \left( c - \frac{\beta_1 c}{2} \right) + A'_s E_s \frac{\varepsilon_c (c - d')^2}{c} + E_c b \frac{\varepsilon_c (h - c)^3}{3c} + A_s E_s \frac{\varepsilon_c (d - c)^2}{c} = M_{ext}, \quad (12)$$

and in the post-yield stage, are

$$\alpha_1 f'_c \beta_1 c b + A'_s E_s \frac{\varepsilon_c (c - d')}{c} - A_s \left[ f_y + E_{sp} \left( \frac{\varepsilon_c (d - c)}{c} - \frac{f_y}{E_s} \right) \right] = 0. \quad (13)$$

$$\alpha'_c f'_c \beta_1 c b \left( c - \frac{\beta_1 c}{2} \right) + A'_s E_s \frac{\varepsilon_c (c - d')^2}{c} + A_s (d - c) \left[ f_y + E_{sp} \left( \frac{\varepsilon_c (d - c)}{c} - \frac{f_y}{E_x} \right) \right] = M_{ext}, \quad (14)$$

Then, if the strain is higher than the yield strain in the compression steel reinforcement

$$A_s 'E_s \frac{\varepsilon_c (c - d')}{c}. \quad (15)$$

In Eqs. (13) and (14), it is required to be used by the term

$$A_x^r \left[ f_y + E_{xp} \left( \frac{\varepsilon_c (c - d')}{c} - \varepsilon_{xy} \right) \right]. \quad (16)$$

The cracking moment  $M_{cr}$  is obtained by Eq. (17), based on the CSA standards [13]

$$M_{cr} = f_r \left( \frac{l_y}{y} \right). \quad (17)$$

$I_g$  and  $y_t$  maybe determined using sectional dimensions and material parameters based on solid mechanics concepts, such as symmetries and shear stresses. Fig. 3 shows different types of cracks in RC beams, such as inclined horizontal web cracks, web cracks, and bottom-flange Y-shaped cracks, including 1) flexural crack, 2) torsion crack, and 3) shrinkage crack.

## 1.4 | Objective of Study

The three samples in group A were treated to three different loads of prolonged loading. As indicated in Table 2, the corroded samples in group B were subjected to three load levels and three current densities. All the beams were loaded 150 days after casting to minimize the impact of concrete creep. To examine their flexural behaviour, we investigated 3 RC beams exposed to enhanced corrosion and another set treated to natural corrosion. To determine how the corrosion process affects the flexural behaviour of the RC beams, the test findings from samples that had been corrupted naturally and quickly were compared. The test findings were included in the Neural Network (NN) model to speed up the accuracy calculation and validate the numerical

results using a realistic model for residual load-bearing capacity. The Finite Element Analysis (FEA) material behaviour models have included all the outputs from the hybrid ANN-SVM.

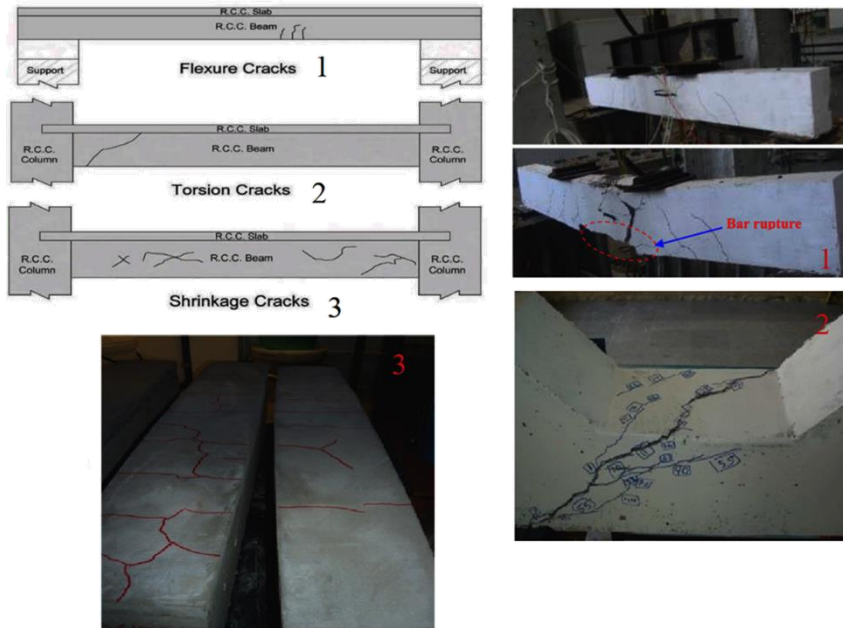


Fig. 3. Different types of cracks in RC beam.

## 2 | Methodology

### 2.1 | Material

Tables 1 and 2 show the characteristics of fine aggregate (sand) (7-30mm), natural coarse aggregate, recycled aggregate, and cement. In this investigation, the cement employed is Portland cement [14]. An 1850 mm-long sustained loading system beam was subjected to four-point bending at 500 mm in the moment region. Weights were suspended from a lever beam and applied to the samples. Two lever arms were employed to increase the suspended weight to the midway of the dispersed beam. Lever arm I was utilized to magnify a hung weight  $G$  from point A to point B. Load  $N$  at point B equals  $l_1 \cdot G$ . Point B's load  $N$  is equal to  $l_1 G$ . One of the three holes might be point A. The value of  $l_1$  maybe 8, 9, or 10 when the weight was suspended from the various holes. Lever arm II multiplied the load  $F$  from point C to point B, resulting in  $F = 8 N$ . As a result, the load at point C on the spread beam might be up to 70, 80, or 90 times greater than the suspended weight  $G$  at point A after multiplying the action of two lever arms.

Table 1. Properties of cement.

Property	Value
Type and class	P.O42.3
Sa m <sup>2</sup> kg <sup>-1</sup>	368
IFT setting times (min)	195/233
LI (%)	1.64
3-day FL (MPa)	5.7/30.45

Table 2. Fine aggregate Properties.

Property	Value
Fineness modulus	2.72
Apparent density (kgm <sup>-3</sup> )	2569
Bulk density (kgm <sup>-3</sup> )	1238
Grain grading	II

## 2.2 | Neural Network

The current NN model was created by training and testing empirical values for 100 corroded concrete members accessible in the literature. The input data values for the NN model are indicated in *Table 3*, which displays the statistical outcomes for the ANN-SVM model. Many fields effectively use NNs, often in conjunction with other AI methods. A network that could categorize standard photos may be used in the following situations: quality assurance determines if metal welding meets the required standards. There are benefits and drawbacks to each network topology and algorithm [15]. A NN is applied to roughly replicate the neuron system and human brain. In essence, NNs are made up of processing components that are closely interconnected. In other words, multi-layer perceptron technology is often used for NN. Layer components are connected by weights ( $w$ ) and are often used in feed-forward NNs.

### 2.2.1 | ANN development

Artificial Neural Networks (ANN) can handle uncertainty concerns and take the role of conventional modelling and simulation techniques. Through the optimization process, the goal function, which was set as the beam's mass at first and got worse if the stress and deformation limits were broken, was to be made as small as possible.

$$f(x) = \text{mass.} \quad (18)$$

The objective function is penalized by *Eq. (19)* if the stress constraint is violated

$$f(x) = f(x) + 10f(x) \left( \frac{(\sigma_{\max} - \sigma_L)}{\sigma_L} \right). \quad (19)$$

Also, in case of violation of the displacement constraint, the objective function is penalized by

$$f(x) = f(x) + 10f(x) \left( \frac{(u_{\max} - u_L)}{u_L} \right). \quad (20)$$

### 2.2.2 | SVM development

Support Vector Machine (SVM) will be applied using the data mining module's machine learning option. A train data subset will make up 75% of the file, while a test data subset will make up 25%. The error function will then be recognized, and SVM type 2 will be specified

$$\frac{1}{2} w^T w - C \left[ v\varepsilon + \frac{1}{N} \sum_{i=1}^N (\zeta_i + \zeta_{i'}) \right]. \quad (21)$$

Which minimizes the entity to

$$\begin{aligned} [w^T \phi(x_1) + b] - y_i &\leq \varepsilon + \zeta_i, \\ y_i - [w^T \phi(x_1) + b_i] &\leq \varepsilon + \zeta_{i'}, \\ \zeta_i, \zeta_{i'} &\geq 0, \\ i &= 1, \dots, N, \varepsilon \geq 0. \end{aligned} \quad (22)$$

Then, the SVM is obtained, so Sigmoid needs to define the extreme values.

$$K(X_i, X_j) = \tanh(\gamma X_i \cdot X_j + C). \quad (23)$$

$K(X_i, X_j) = \varphi(X_i) \cdot \varphi(X_j)$ , meaning that SVM shows input and output values in multidimensional space through transformation  $\varphi$  [16].

Given the dataset size in this instance, we tested our classifiers using the cross-validation approach. The data is divided into ten folds of equal size at random. We chose six samples from the control group and six samples from the test group for each fold. The next step involves using one fold for testing and the remaining nine for validation. This method is repeated ten times, each iteration holding out a unique data fold for validation while the remaining folds are utilized for learning. The suggested study identifies the flexural behavior of a



corroded concrete beam prediction system using an SVM and ANN combination. In SVM, the decision boundary would be a hyperplane between the collection of data points.

## 2.3 | Finite Element

The Finite Element Method (FEM) is a computational method used to approximate the behaviour of a physical system. It involves dividing the system into smaller, simpler sub-regions called finite elements and solving equations for each element to obtain an approximate solution for the system's overall behaviour. Nodal values may be used to retrieve values from inside FMs. The essential stages of the FM solution approach are listed below:

- I. Problem definition: define the problem statement, including boundary conditions, loads, and material properties.
- II. Mesh generation: divide the problem domain into smaller and simpler finite elements. The mesh must be generated to represent the geometry and accurately preserve the structure's continuity.
- III. Element properties: define the element properties such as stiffness matrix, mass matrix, and damping matrix.
- IV. Assembly: combine the element matrices by assembling the global stiffness matrix, mass matrix, and damping matrix.
- V. Boundary conditions: apply the boundary conditions to the global system of equations.
- VI. Solution: solve the system of equations using numerical methods, such as the direct method, iterative method, or eigenvalue method.
- VII. Post-processing: analyze and visualize the results, such as stresses, strains, deflections, and natural frequencies [17].

### 2.3.1 | Formulation of finite element equations

The Galerkin approach of FM formulation is shown using a numerically one-dimensional example [18]

$$a \frac{d^2 u}{dx^2} + b = 0, \quad 0 \leq x \leq 2L. \quad (24)$$

With boundary conditions

$$\begin{aligned} u|_{x=0} &= 0, \\ a \frac{du}{dx} \Big|_{x=2L} &= R. \end{aligned} \quad (25)$$

$u$  = an unknown solution

The element with two nodes and the function  $u(x)$  as

$$\begin{aligned} u &= N_1 u_1 + N_2 u_2 = [N]\{u\}, \\ [N] &= [N_1 \quad N_2], \\ \{u\} &= \{u_1 \quad u_2\}. \end{aligned} \quad (26)$$

$$\begin{aligned} N_1 &= 1 - \frac{x - x_1}{x_2 - x_1}, \\ N_2 &= \frac{x - x_1}{x_2 - x_1}. \end{aligned} \quad (27)$$

Where  $N_i$  is the shape function utilized to interpolate  $u(x)$  through its nodal values. Nodal values  $u_1$  and  $u_2$  are defined from the discrete global equation system. In the differential equation, after substituting  $u$  defined through its shape functions and nodal values, it could be

$$a \frac{d^2}{dx^2} [N]\{u\} + b = \psi. \quad (28)$$

$\psi$  = a nonzero residual because of the approximate function within FM.

For residual minimization, the Galerkin approach uses the following equation's terms multiplied by form functions, then integrates over the element to get zero

$$\int_{x_1}^{x_2} [N]^T a \frac{d^2}{dx^2} [N] \{u\} dx + \int_{x_1}^{x_2} [N]^T b dx = 0, \quad (29)$$

$$\int_{x_1}^{x_2} \left[ \frac{dN}{dx} \right]^T a \left[ \frac{dN}{dx} \right] dx \{u\} - \int_{x_1}^{x_2} [N]^T b dx - \left\{ \begin{matrix} 0 \\ 1 \end{matrix} \right\} a \frac{du}{dx} \Big|_{x=x_2} + \left\{ \begin{matrix} 1 \\ 0 \end{matrix} \right\} a \frac{du}{dx} \Big|_{x=x_1} = 0. \quad (30)$$

Usually, such a relation for an FM is shown as follows:

$$\begin{aligned} [k] \{u\} &= \{f\}, \\ [k] &= \int_{x_1}^{x_2} \left[ \frac{dN}{dx} \right]^T a \left[ \frac{dN}{dx} \right] dx, \\ \{f\} &= \int_{x_1}^{x_2} [N]^T b dx + \left\{ \begin{matrix} 0 \\ 1 \end{matrix} \right\} a \frac{du}{dx} \Big|_{x=x_2} - \left\{ \begin{matrix} 1 \\ 0 \end{matrix} \right\} a \frac{du}{dx} \Big|_{x=x_1}. \end{aligned} \quad (31)$$

In solid mechanics,

$[k]$  = stiffness matrix.

$\{f\}$  = load vector.

The load vectors and two FM of length L stiffness matrices could be easily computed:

$$\begin{aligned} [k_1] &= [k_2] = \frac{\alpha}{2} \begin{bmatrix} 1 & -1 \\ -1 & 1 \end{bmatrix}, \\ \{f_1\} &= \frac{\mu L}{2} \begin{Bmatrix} 1 \\ 1 \end{Bmatrix}, \quad \{f_2\} = \frac{\mu L}{2} \begin{Bmatrix} 1 \\ 1 \end{Bmatrix} + \begin{Bmatrix} 0 \\ R \end{Bmatrix}. \end{aligned} \quad (32)$$

The above relations give the equations for the two different FMs. By putting the element equations together, it is possible to get a global equation system for the domain with 2 elements and 3 nodes. The global equation system as a whole is:

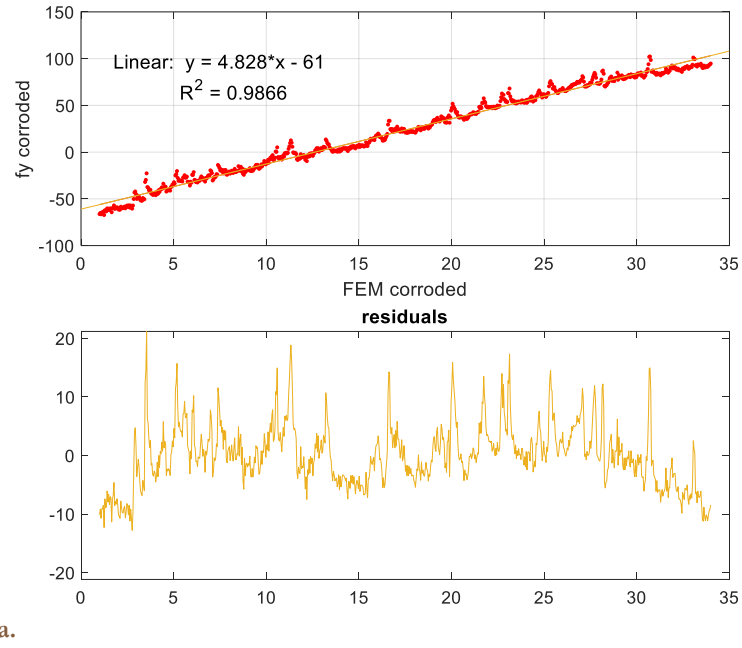
$$\frac{a}{L} \begin{bmatrix} 1 & -1 & 0 \\ -1 & 2 & -1 \\ 0 & -1 & 1 \end{bmatrix} \begin{Bmatrix} u_1 \\ u_2 \\ u_3 \end{Bmatrix} = \frac{bL}{2} \begin{Bmatrix} 1 \\ 2 \\ 1 \end{Bmatrix} + \begin{Bmatrix} 0 \\ 0 \\ R \end{Bmatrix}. \quad (33)$$

It's important to note that the FM method gives exact u values at each node. If the solution you want is quadratic, linear shape functions will give you exact nodal values. Fig. 4 shows the findings of the load-deflection curves of the tested beams. The load-deflection curves of three beams with various positions of corroded stirrups are shown in Fig. 5, with satisfactory agreement between experimental and tested findings.

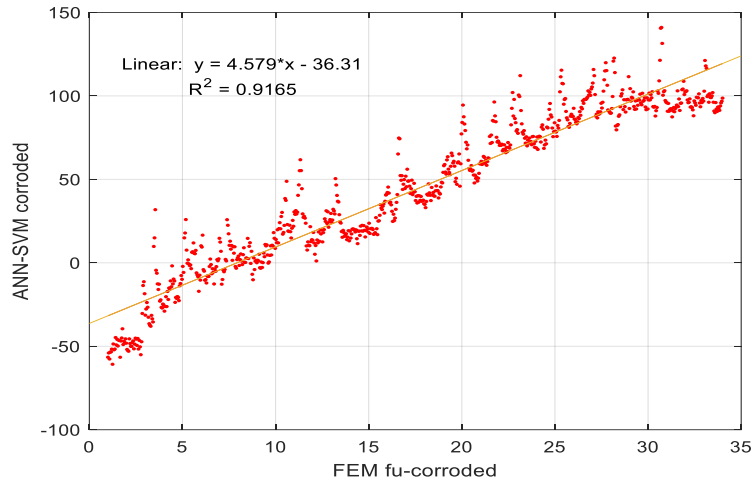
**Table 3. Input variables in this NN analysis.**

Item	Minimum Value	Maximum Value
Corrosion period/days	0	9490
fc'	10.7	63
Tensile steel bars/ mm <sup>2</sup>	78.5	8164
fc' area/ mm <sup>2</sup>	0	2260.8
fy MPa	345	585
Yielding stress of fc' fy'	428	891.25



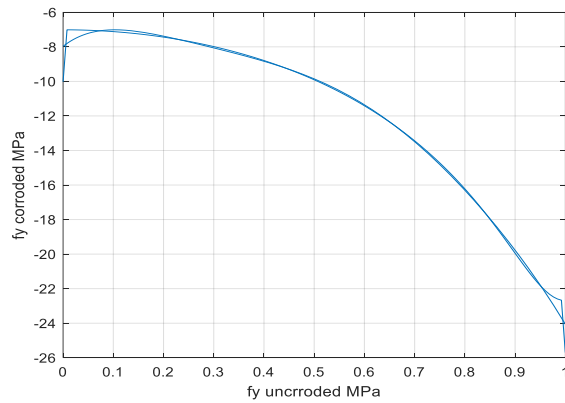


a.

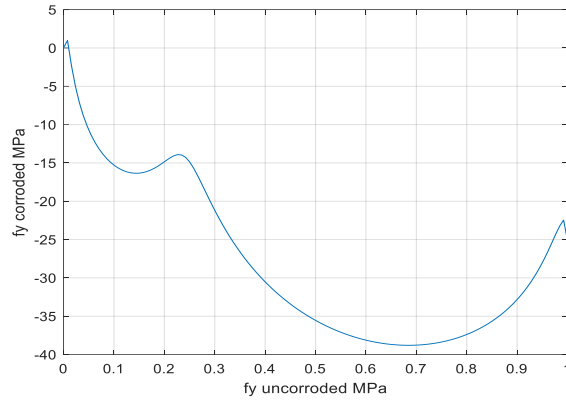


b.

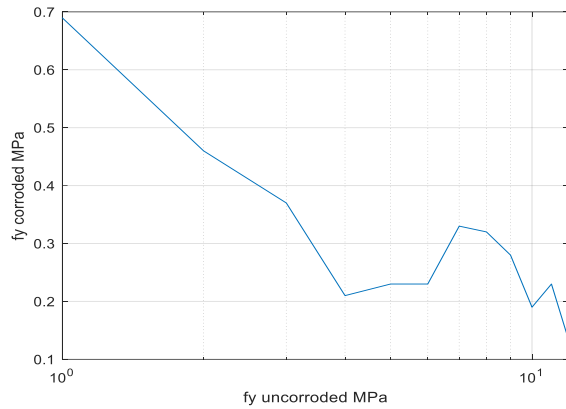
Fig.4. Here are the load-deflection curves of tested beams with 10% to 50% tension reinforcement losses; a) bond strength degradation is less significant than flexural cross-section loss, b) by increasing tension reinforcement cross-section loss, tested beams' load-bearing capacity decreases.



a.



b.



c.

**Fig. 5. ANN-SVM model for input 1: Using an FE model, the ultimate flexural strength of tested beams might well be exactly predicted; a) caption, b) caption.**

The beam B9-MC-MS exhibited the least flexural capacity due to considerable corrosion (approximately 10% weight loss), stirrup corrosion in a halfway span, and an 18.11 per cent decline from the control beam. The maximum load that the beam B9 could support in the test was 32.4 kN, but the maximum load predicted by the FEM results at the same deflection was closer to 35.0 kN. The least reduction in load-carrying capacity is caused by the shear span stirrup corrosion on beam B7-MC-SS (37.0 kN in test versus 39.0 kN in FEM). The beam B3-MCFS's flexural capacity was 7.69 per cent lower than the control beam's.

### 3 | Result and Discussion

Numerous performance measures, such as correlation coefficient (R), Root Mean Squared Error (RMSE), and others, have been published in the open literature. In practice, a set of criteria determines if a given ML model is appropriate. ANNs, genetic programming, and others are a few of these methods. The PFEMs collected here are a subset of metrics based on point distance estimation methods that mostly use subtraction or division operations. These metrics cover the fundamental operations A-P or P/A, with additional options like absoluteness or squareness. The most often used literary metrics are those listed below. Eighty per cent of the data is completely separated for the training component, and twenty per cent is completely separated for the testing part of the model (ANN-SVM) to assess performance. As performance measures, the determination coefficient (R<sup>2</sup>), RMSE, and r were used for statistical models.

$$r = \frac{N(\sum_{i=1}^N O_i \cdot P_i) - (\sum_{i=1}^N O_i) \cdot (\sum_{i=1}^N P_i)}{\sqrt{(N \sum_{i=1}^N O_i^2 - (\sum_{i=1}^N O_i)^2) \cdot (N \sum_{i=1}^N P_i^2 - (\sum_{i=1}^N P_i)^2)}} \quad (34)$$

$$R^2 = \frac{[\sum_{i=1}^N (O_i - \bar{O}) \cdot (P_i - \bar{P})]^2}{\sum_{i=1}^N (O_i - \bar{O}) \cdot \sum_{i=1}^N (P_i - \bar{P})} \tag{35}$$

$$RMSE = \sqrt{\sum_{i=1}^N \frac{1}{N} (O_i - P_i)^2} \tag{36}$$

N = the number of training or testing samples.

$O_i$  = observed values in sample i.

$P_i$  = predicted values in sample i.

$\bar{O}$  = the mean observed values.

$\bar{P}$  = the mean predicted values.

### 3.1 | Discussion of Corroded

As seen in *Fig. 5*, an accelerated corrosion instrument was used to simulate corrosion using electrochemical techniques and wet-dry cycles. The device for accelerated corrosion could give DC electricity to 8 samples simultaneously without affecting any of them. Though theoretical formulas have been presented to determine the corroded condition of samples, the test findings are still variable due to differences in material, current density, and test duration. The text describes a study investigating rebar corrosion behaviour in RC beams. Cracks were the most noticeable effect of the corrosion process, and the width of these cracks was used as the primary criterion for evaluating the degree of corrosion. Half-cell potential and sectional loss rate of rebars were also used to detect corrosion. After the corrosion tests, the rebars were removed, and their section loss rates were assessed by measuring the cross sections with the greatest area loss. AUTOCAD was used to design the section forms and calculate their area. The text suggests that a static stress test was conducted on the beams, and some rebars exhibited plastic necking deformation.

### 3.2 | Analysis of ANN-SVM

This study aimed to create bankruptcy prediction models and assess the outcomes of ANN and SVM. The models were developed: 1 SVM and 1 NN. Consequently, they were compared to one another. The most effective model that may be used in practice is NN 2.MLP 22-9-2 (NN code C++ forms). The functioning of the ANN-SVM model concerning prior performance metrics was assessed in both the training and testing phases after investigating the model's related parameters. The goodness of fit was the major metric for comparing the two models in terms of their predictive power. The RMSE values of both models were compared to compare the regression parameters, and the model with the closest value to 0 had the best performance.

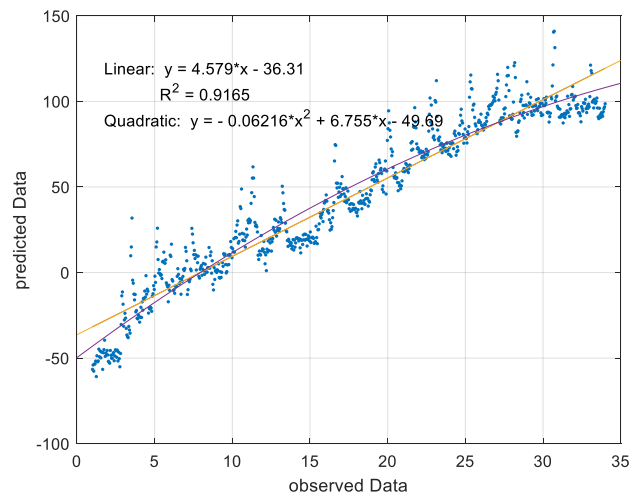


Fig. 6. Distribution of data in the hybrid ANN-SVM.

Since the findings were so near zero, comparing the RMSE of the two phases in the model might demonstrate improved performance in forecasting the flexural behaviour of corroded concrete beams (lowest RMSE) (Fig. 7). ANN-SVM had the greatest performance in the test phase when comparing the RMSE of the train and test phases (0.657, 0.577) (Fig. 6). Additionally, the model's R-square value is (0.9165) (highest R<sup>2</sup>) that shows the accuracy of the model.

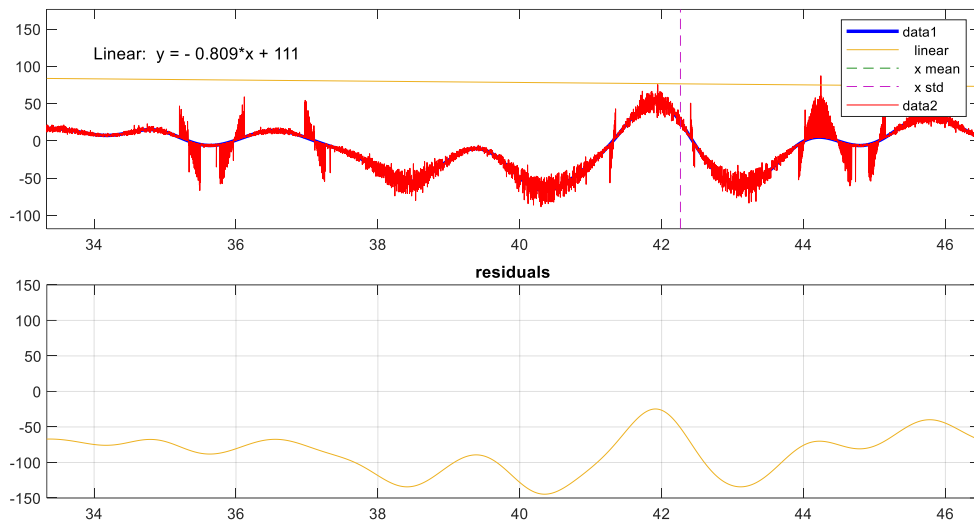


Fig. 7. RMSE of the hybrid, horizontal axis is the data number; the vertical axis is the RMSE values.

## 4 | Conclusions

This study models the effects of stirrup corrosion on the flexural capacity of eight corroded RC beams and explores those implications. An ANN-SVM software-based FEA method was developed to describe the structural responses of corroded beams considering two separate inputs: 1) without stirrups in the flexural span and 2) with corroded stirrups at varied places. The FE model is verified by contrasting the experimental and numerical results of the load-deflection curves. Moreover, a parametric simulation was run to assess how the reduction in bond strength and the shrinking of tension reinforcement cross sections affected the beam's flexural strength. As a result of our research, we have come to the following key conclusions: the flexural capacity of the corroded beams can be predicted with high precision thanks to the finite element model utilized in this investigation, which accounts for corrosion damage to the reinforcement, concrete, and steel-concrete connection. The finite element study showed that the flexural behaviour of a corroded beam was affected by stirrup corrosion, namely by a reduction in the middle span deflection. If you have a corroded beam with locally corroded stirrups, you may see a significant weight loss, on the order of 30 per cent, in the shear span due to the corrosion. However, when homogeneous corrosion is applied to U-type stirrups, there is no discernible difference in flexibility and flexural capacity between corroded and control beams. The outcomes of an experiment could be better understood with the use of a soft computing model.

## Author Contributions

The authors contributed equally to the research.

## Funding

The research did not receive any funding.

## Data Availability

The data used in this study are available upon request from the corresponding author.

## Conflict of Interest

The authors declare no conflict of interest.

## References

- [1] Zhang, W., Shang, D., & Gu, X. (2006). Stress-strain relationship of corroded steel bars. *Tongji daxue xuebao/journal of tongji university*, 34(5), 586–592.
- [2] Zhang, W., Zhang, H., Gu, X., & Liu, W. (2018). Structural behavior of corroded reinforced concrete beams under sustained loading. *Construction and building materials*, 174, 675–683.
- [3] Mehta, P. K. (1994). Concrete technology at the crossroads--problems and opportunities. *Special publication*, 144, 1–30.
- [4] Ballim, Y., & Reid, J. C. (2003). Reinforcement corrosion and the deflection of RC beams---an experimental critique of current test methods. *Cement and concrete composites*, 25(6), 625–632.
- [5] Alonso, C., Andrade, C., Rodriguez, J., & Diez, J. M. (1998). Factors controlling cracking of concrete affected by reinforcement corrosion. *Materials and structures*, 31(7), 435–441.
- [6] Andrade, C., & Alonso, C. (2001). On-site measurements of corrosion rate of reinforcements. *Construction and building materials*, 15(2–3), 141–145.
- [7] Branson, D. E. (1976). *Deformation of concrete structures*. McGraw-Hill Companies.
- [8] Kemp, E. L., & Wilhelm, W. J. (1979). Investigation of the parameters influencing bond cracking. *Journal proceedings*, 76(1), 47–72.
- [9] Saifullah, M., & Clark, L. A. (1994). Effect of corrosion rate on the bond strength of corroded reinforcement. *Corrosion and corrosion protection of steel in concrete*, 1, 591–602.
- [10] Rodriguez, J., Ortega, L. M., & Casal, J. (1994). Corrosion of reinforcing bars and service life of reinforced concrete structures: corrosion and bond deterioration. *International conference on concrete across borders* (Vol. 2, pp. 315–326). Odense, Denmark: Taylor & Francis, Abingdon, UK.
- [11] Walraven, J. C., & Bigaj-van Vliet, A. J. (2008). A new future-oriented model code for concrete structures. *Proceedings of the international fib symposium 2008 - tailor made concrete structures: new solutions for our society* (p. 140). London: Taylor & Francis Group. DOI: 10.1201/9781439828410.ch101
- [12] Collins, M. P., & Mitchell, D. (1987). *Prestressed concrete basics*. Canadian prestressed concrete institute.
- [13] Association, C. S., & of Canada, S. C. (1994). *A23.3-94 Design of concrete structures: structures (design)*. The Association.
- [14] Zou, Z., Yang, G., & Su, T. (2020). Analytical model to predict residual flexural capacity of recycled aggregate concrete beams with corroded longitudinal rebars. *Advances in materials science and engineering*, 2020. DOI:10.1155/2020/3079892
- [15] Jensen, C. A., Reed, R. D., Marks, R. J., El-Sharkawi, M. A., Jung, J.-B., Miyamoto, R. T., ... , & Eggen, C. J. (1999). Inversion of feedforward neural networks: algorithms and applications. *Proceedings of the IEEE*, 87(9), 1536–1549.

- [16] Horak, J., Vrbka, J., & Suler, P. (2020). Support vector machine methods and artificial neural networks used for the development of bankruptcy prediction models and their comparison. *Journal of risk and financial management*, 13(3), 1-15.
- [17] Horak, J., Vrbka, J., & Suler, P. (2020). Zieli, T. G. (1992). Introduction to the finite element method. *Journal of risk and financial management*, 13(3), 1–15. <https://www.mdpi.com/1911-8074/13/3/60/pdf>
- [18] Zieli, T. G. (1992). *Introduction to the finite element method*.  
[http://bluebox.ippt.pan.pl/~tzielins/doc/ICMM\\_TGZielinski\\_IntroFEM.Slides.pdf](http://bluebox.ippt.pan.pl/~tzielins/doc/ICMM_TGZielinski_IntroFEM.Slides.pdf)